ETEAPOT EDM Benchmark-IV: Code comparisons: ETEAPOT, MAPLE, Lebedev, and Runge-Kutta

R.M.. Talman and J.D. Talman

December 5, 2019

Abstract

This chapter compares the results of various lattice programs for Valeri Lebedev's all-electric proton EDM lattice, (here referred to as `E_ValLeb2-sl4-RF.sxf`) a full-scale "Holy Grail" lattice adopted for the RSI EDM paper[1]. As required for EDM measurement sensitivity, this lattice has significantly stronger focusing horizontally than vertically.

For transverse optics the agreement among three independent analyses, two based on the Wollnik transfer matrix formalism, one using the ETEAPOT lattice simulation code, is excellent. Plots and tables bear this out.

The comparison of longitudinal dynamics is somewhat less satisfactory. A crude comparison between ETEAPOT and Runge-Kutta analysis of longitudinal dynamics in a previous benchmark lattice `E_BM_Z-RF.sxf` is given. Factors making such comparisons delicate are discussed. The importance of proving beam capture into stable longitudinal buckets is emphasized. In fact, unlike `E_BM_Z-RF.sxf`, attempts to achieve stable capture into the `E_ValLeb2-sl4-RF.sxf` lattice have failed so far. It is not known at present whether this is a property of the lattice, which would be surprising, or a bug in ETEAPOT.

1 Parameters of Benchmark Proton EDM Lattices

Transverse Twiss parameters have been calculated from linearized transfer matrices in two different ways, one described in this report, and referred to as R.M.T., and one from the initial Lebedev report[2] and referred to as V.L. Both of these analyses are based on the Wollnik[7] linearized transfer matrix formalism. As such, they are independent only as regards lattice details, element slicing, and interpretation of the formalism. The third analysis, based on ETEAPOT is here referred to as J.D.T.

The ETEAPOT approach is to perform exact tracking in an approximate lattice, and to reconstruct the Twiss parameters by numerical post-processing the results from tracking a standard bunch of 21 small amplitude particles. Being based on entirely different formalisms, the comparison of ETEAPOT and Wollnik-based results can provide a stringent test of our understanding of the proposed proton EDM lattice.

Comparisons of transverse lattice parameters are given in Table 1. The R.M.T and J.D.T. analyses are based on lattice file `ValLeb2-sl4.sxf` which has been reconstructed from the original Lebedev[2] report. The lattice is simple enough, and the Lebedev report careful and thorough enough, that this reconstruction could be performed with little ambiguity. The only significant uncertainty was that only the ratio of quadrupole fields GDD/GFF, rather than the absolute quad strengths (i.e. inverse focal lengths) is given in the report [2]. The tunes Q_x and Q_y are given, however, and, from these, the absolute (half-)quad strengths qFh and qDh have been determined.

Table 1: Transverse lattice parameters of the proton EDM lattice proposed by Valeri Lebedev[3], as evaluated in three independent ways. This lattice (here referred to as `ValLeb2-sl4.sxf`) can serve as an up-to-date "Holy Grail" lattice.

Analysis method	author	half-quad strength qFh	quad ratio GDD/GFF or qDh/qFh	horz. tune Q_x	vert. tune Q_y	max. horz. β_x	min. horz. β_x	max. vert. β_y	min. vert. β_y
		1/m				m	m	m	m
linear tr.mat.	V.L.	-0.0307	-0.802	2.32	0.31	29.1	≈ 16	204	≈ 118
MAPLE	R.M.T.	-0.0307	-0.765	2.32	0.315	29.2	15.4	201.8	114.0
ETEAPOT	J.D.T.	-0.0303	-0.765	2.31	0.325	29.2	15.4	196	110.8

In the `ValLeb2-sl4.sxf` latice description file, the "`-sl4`" indicates that the bend elements have been artificially sliced by a factor of four, from about 9 meters to about 2.25 meters. This has been done both for making the physical construction more realistic, and to relieve the burden on ETEAPOT tracking over such long elements. As it happens, ETEAPOT automatically performs a further splitting of a factor of two, to make lattice parameters available at element centers. Also ETEAPOT can perform further splitting in order to represent bend elements having field indices other than $m = 0$ (which corresponds to "cylindrical" bent-planar, parallel electrodes). However for the present study we fix $m = 0$.

Table 1 shows excellent agreement among the three approaches. With qFh constrained to be identical for all studies, the main discrepancy was assuming $m = 0.235$ in the TEAPOT calculation, whereas the Lebedev calculation assumed $m = 0.2$. A discrepancy at least this large can be expected from the fundamental ambiguity in the treatment of electric elements, especially in the comparison between ETEAPOT and Wollnik approaches. As it happens there is essentially no difference in the treatments based on the identical lattice description file, and the entire discrepancy is between V.L. and R.M.T. implementations of the Wollik approach on slightly different lattices. In any case all comparisons are sufficiently good that there can be no doubt the transverse lattice performance will be essentially just as Lebedev has first stated. One must keep in mind, however, that the lattice with unbalanced focusing is quite "high strung". For example, a 1% change in the qDh focal length reduces Q_y from 0.3 to 0.0 (where the lattice becomes unstable).

R.M.T. linear transfer matrix Twiss functions are compared to J.D.T. ETEAPOT Twiss functions in Figures 1 and 2. V.L. linear transfer matrix Twiss functions are compared to ETEAPOT Twiss functions in following figures. There is excellent agreement in all cases.

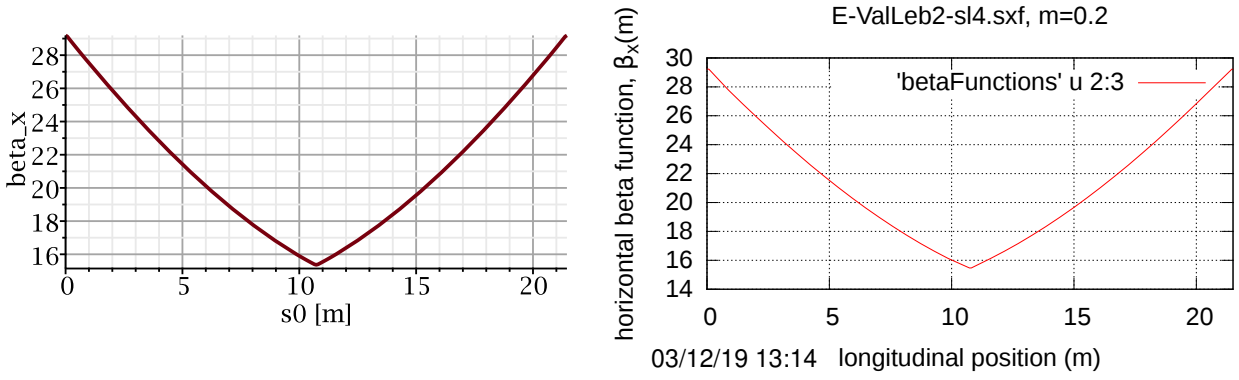

Figure 1: Proton EDM Lattice β_x functions as determined by MAPLE linear transfer matrix formalism, on the left, and by ETEAPOT, on the right.

Figure 3, copied directly from the original Lebedev report, gives his beta functions and dispersions.

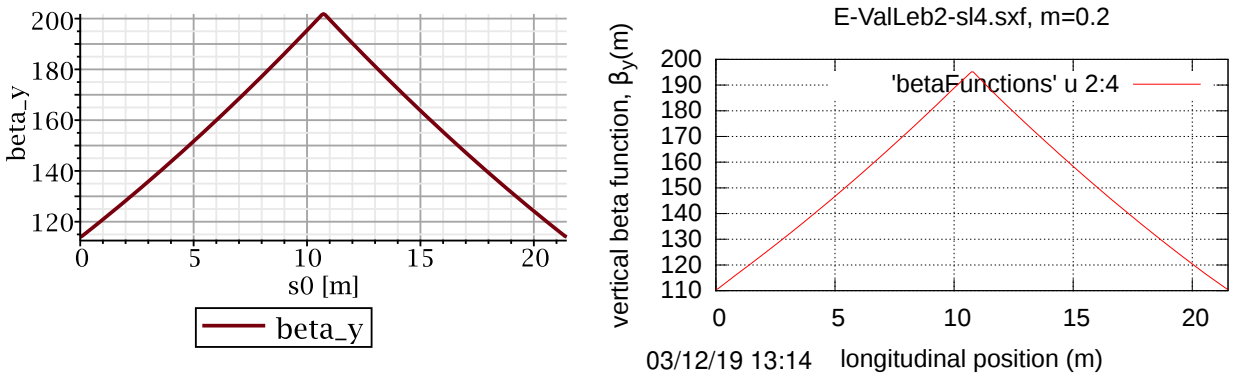

Figure 2: Proton EDM Lattice β_y functions as determined by MAPLE linear transfer matrix formalism, on the left, and by ETEAPOT, on the right.

The beta functions can be compared with MAPLe and ETEAPOT results shown in Figures 1 and 2.

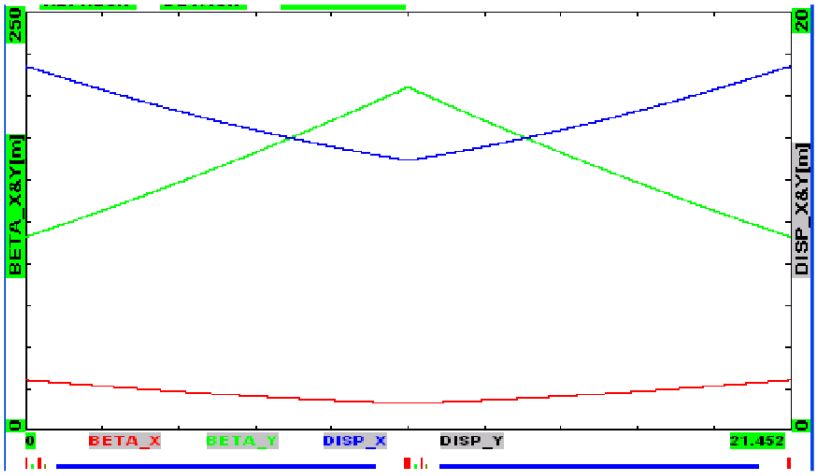

Figure 3: Proton EDM Lattice β functions as determined by Valeri Lebedev[2]. Also shown is the dispersion function.

1.1 Fractional off-momentum notation

To call attention to one complication accompanying the introduction of electric elements, we define here multiple fractional longitudinal offset variables: starting with "fractional rigidity offset" δ_R and "fractional total energy offset" δ. For magnetic lattices the latter quantity will also be referred to as δ_{UAL}; it is the fractional longitudinal phase space coordinate definition used by MAD and UAL (and now also by ETEAPOT). Its definition is

$$\delta_{UAL} = \frac{\mathcal{E} - \mathcal{E}_0}{p_0 c}, \tag{1}$$

where p_0 is the design momentum, $\mathcal{E} = \gamma m_p c^2 + eV(\mathbf{x})$ is the total energy and γ is the conventional relativistic parameter. The "mechanical energy" is $\gamma m_p c^2$. For magnetic elements, because γ is conserved, this definition is applicable either inside or outside bend elements. For electric elements (for which it is $\mathcal{E}$

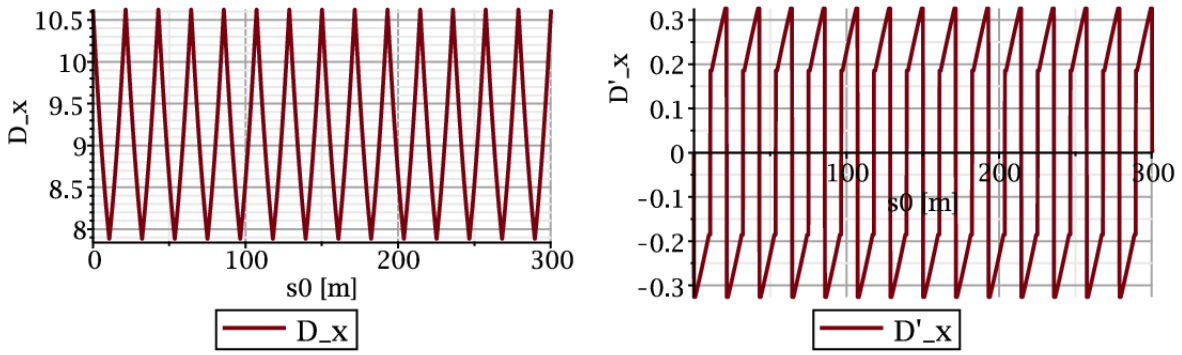

Figure 4: Proton EDM Lattice dispersion D_{UAL} and dispersion slope D'_{UAL} as determined by MAPLE. Note that definitions of "dispersion function" differ for different formalisms. This is discussed in Section 1.1.

that is conserved) γ varies (discontinuously at step function voltage cahnges) as a particle moves between regions of different electric potential.

It needs to be agreed that, for comparing differently derived results, it is parameter values *outside* electric elements that should be compared (even if the ring is mainly bends) and particles are *rarely* "outside bends".) To avoid confusion, quantities can be specified with superscript "O" for "outside" or "I" for "inside".

The defining equation for "fractional rigidity offset" δ_R is

$$R = R_0(1 + \delta_R), \tag{2}$$

where R_0 is the radius of the design circular orbit and R is the radius of the orbit (locally circular) of the offset particle in the same local field. By this definition δ_R is identical to (or at least very close to) Wollnik's[7] Δ, which he defines in his Section 4.1.1.2. (For a uniform electric or any magnetic field the "at least very close to" qualification is unnecessary. For a non-uniform electric field one has to follow Wollnik's definitions more carefully.

ETEAPOT uses δ_{UAL}, defined above as the sixth phase space component of a particle being tracked through a lattice. (However, δ_{UAL} cannot be used to differentiate between orbits of different radii inside a bend element having electric field proportional to $1/r$; this is because the dependence of radius on mechanical energy is singular. (Regrettably the optimal EDM bend field varies approximately as $1/r$.) Outside electrical field regions,

$$\delta_{UAL} = \frac{(\gamma^O - \gamma_0)m_p c^2}{p_0 c}. \tag{3}$$

In drifts (or magnets) this is identical to Eq. (1).

By design, in all-electric rings, the electric potential is *everywhere* zero on the design orbit. Element errors will cause the central closed orbit to deviate somewhat from the design orbit. Except for this $\gamma^O = \gamma^I$ on the central closed orbit.

At arbitrary, inside or outside, bends, the longitudinal deviation variable δ_{UAL} used in MAD and UAL is defined by

$$\delta_{UAL} = \frac{\Delta\mathcal{E}_{\mathrm{mech.}}}{p_0 c} = \frac{m_p c^2 \Delta\gamma}{p_0 c}. \tag{4}$$

Here $\mathcal{E}_{\mathrm{mech.}} = \gamma m_p c^2$ stands for the "mechanical energy", which is the total energy minus the potential energy. One then finds

$$\Delta(pv) = m_p \Delta(\gamma v^2) = m_p c^2 \Delta\Big(\gamma - \frac{1}{\gamma}\Big) = \Big(1 + \frac{1}{\gamma_0^2}\Big)\frac{p_0 v_0}{\beta_0}\,\delta_{UAL}, \tag{5}$$

and

$$pv \approx p_0 v_0 \left(1 + \left(1 + \frac{1}{\gamma_0^2}\right) \frac{1}{\beta_0}\, \delta_{UAL}.\right) \tag{6}$$

As defined here, the fractional rigidity deviation Δ relates the radius of curvature r of a deviant particle to the radius of curvature r_0 of an on-momentum particle, both in the same uniform field;

$$r = r_0\,(1 + \Delta). \tag{7}$$

Δ is therefore related to the MAD/UAL momentum deviation factor δ by[1]

$$\Delta = \left(1 + \frac{1}{\gamma_0^2}\right) \frac{1}{\beta_0}\, \delta_{UAL} \quad \left(= 2.744\, \delta_{UAL}\right). \tag{8}$$

for the all-electric proton EDM experiment.

This (surprisingly large) factor accounts for much of the large difference in Lebedev and ETEAPOT determinatons of ring dispersion.

2 Comparison of Longitudinal Dynamics

Though transverse dynamics in all-electric proton EDM rings is now completely under control, the same cannot be said for longitudinal dynamics. From now on it will be important, appropriate, and possible, to concentrate more on longitudinal dynamics.

Initial benchmark comparisons of results of ETEAPOT and Runge-Kutta tracking showed seemingly contradictory results. For example ETEAPOT tracking[5] showed long term instability limiting the dynamic aperture to be about an order of magnitude less than given by Runge-Kutta tracking[6]. We have now realized that this inconsistency may be partially understood in terms of the vastly disparate peak RF voltages that were being assumed for the two studies. In both cases harmonic number $h = 100$ was assumed, but the largest peak RF voltage in the ETEAPOT study was 5 KV, whereas, in the Runge-Kutta study the peak voltage was 1 MV. This factor of 200 difference can certainly be expected to affect the comparison. Extending the range of RF voltages in the ETEAPOT study to 0.1 MV (above which instability results) one obtains the comparison shown in Figure 5. This is not intended as evidence of "agreement" between the results; rather it is intended as a beginning on the route to eventual, more controlled, comparison. Complications in performing such comparisons are discussed next.

In Figure 5 the three Runge-Kutta traces correspond to initial x-amplitudes of -1 cm (blue), 0 (green), and +1 cm (red), all with $\Delta p/p = 2 \times 10^{-4}$. (For the ETEAPOT plot, for the same three cases, in the same order, the colors are red, green, blue, blue.) The x-ranges of both plots are about the same. For the Runge-Kutta plot the RF voltage was 1 MV. For the ETEAPOT plot the RF voltage was 0.1 MV (approximately the highest voltage for which the particles could be captured into stable buckets). This comparison is discussed (and qualified) further in the text. Though it has been stated that the same lattice (namely `E_BM_Z-RF.sxf`) has been used in the ETEAPOT/Runge-Kutta comparison, this is only approximately true, especially as regards the (weak) vertical focusing needed to preserve vertical stability. Furthermore the m-values are slightly different. These blemishes are not expected to be significant.

The ETEAPOT/Runge-Kutta comparison in Figure 5 is as close as it is only because various empirical adjustments (for example resolving ambiguous lattice details to make the plots look more similar) have been made. While it has been easy to specify transverse-sensitive lattice conditions unambiguously it is harder to specify longitudinal conditions. The effective beta-functions and dispersions are unkown for the Runge-Kutta plot, which probably accounts for the twice greater transverse range of the Runge-Kutta orbits. Also there is ambiguity as to whether the beam is specified inside or outside electric field regions; the change in kinetic energy in passing from inside to outside affects this specification. It is also important to specify where in the ring the RF cavity is situated, as beam capture depends on this. If the RF cavity

[1]For comparison with Wollnik's Eq. (4.58c) one should note that Wollnik's $\delta_K = (K - K_0)/K_0$ is a fractional kinetic energy, while our MAD/UAL $\delta = (E - E_0)/p_0 c$. The numerators are the same but our denominator is bigger by $p_0 c/K_0 = 3.01$.

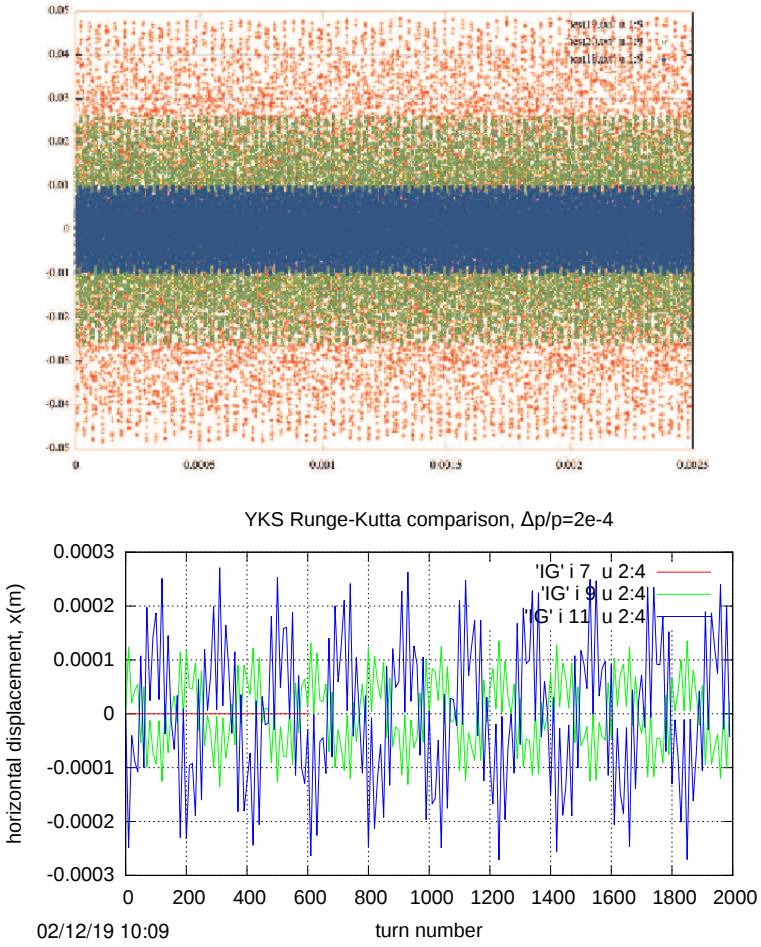

Figure 5: Comparison of (Figure 18 of reference[6]) Runge-Kutta tracking (above) with ETEAPOT tracking (below).

is at the beginning or end of the lattice (as is convenient for such studies) it is essential to know whether the beam is injected just before or just after the RF. More generally, the specification of longitudinal performance depends on the full, six-dimensions in phase space, of the initial bunch distribution.

The fine grain structure of the ETEAPOT and Runge-Kutta plots in Figure 5 are similar. By counting red peaks one finds the "synchrotron tune" Q_s of this granularity to be $Q_s = 9.9/2000 = 0.005$ for the ETEAPOT plot. (Though it is not possible to infer it from the fuzzy plot) this is the same for all three traces; see Figure 6. For the outermost (red) Runge-Kutta plot there are 14 periods in 0.0005 s, which corresponds to 357 turns. This yields $Q_s = 14/357 = 0.039$. Again, the blue and green peaks are too fuzzy to be counted in the figure as reproduced here. But the plots in the original report[6] are clearer, and there seem to be 15.5 green peaks over the same interval that there are 14 red peaks. If true, it would imply the red and green particles have not been captured in the same bucket. This should be checked.

To illustrate these issues further, the left plot of Figure 6 shows the longitudinal phase space evolution corresponding to the ETEAPOT data on the bottom in Figure 5. The most essential aspects of longer run durations of this figure is that the longitudinal phase space orbits are identical in the three cases, and the particles are limited to the longitudinal range from -0.019 m to +0.019 m. In other words, the particles have been captured into a stable bucket. This limitation, specific to capture into a stable bucket, cannot easily be inferred from Figure 5.

From the comparison of Figures 5 and 6 one sees also that the distribution in transverse amplitude x

is strongly correlated with the range in energy spread $\Delta E/p_o c$. When the three particles were injected (from zero electric potential outside bend elements) their kinetic energies were the same but, inside electric elements, their kinetic energies have become different, both because of the different potentials they had to surmount on entry, and because of the different energies imparted by the RF.

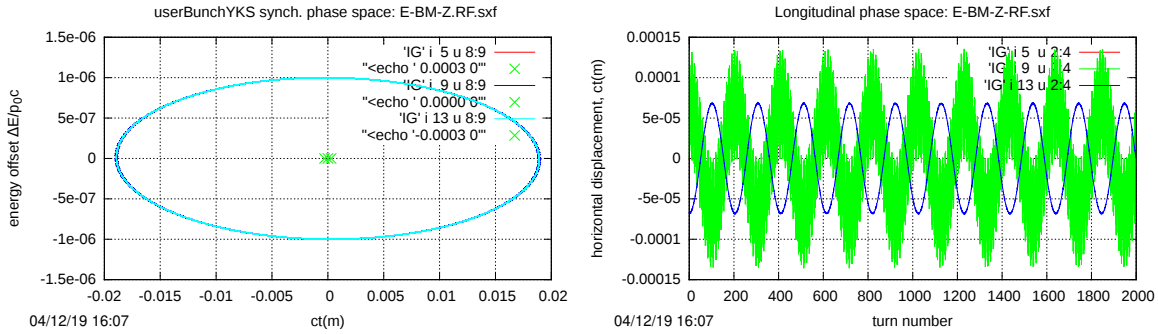

Figure 6: Longitudinal phase space plots corresponding to the ETEAPOT data on the right in Figure 5. The figure on the right checks that the three traces are exactly synchronized, as is required for the particles to be in the same stable bucket.

References

[1] V. Anastassopoulos et al., *A storage ring experiment to detect a proton electric dipole moment,* Review of Scientific Instruments, **87**, 115116 (2016)

[2] V. Lebedev, *Prospects of Strong Horizontal Focusing Electric Ring: Advantages, Disadvantages,* Storage Ring EDM Collaboration Meeting, December 9-10, 2013

[3] J.D. Talman and R.M. Talman, *UAL/ETEAPOT Results (Augmented) for Proton EDM Benchmark Lattices,* BNL internal report, April 29, 2012

[4] J.D. Talman and R.M. Talman, *UAL/ETEAPOT Proton EDM Benchmark Comparisons II: Transfer Matrices and Twiss Functions,* BNL internal report, August 30, 2012

[5] J.D. Talman and R.M. Talman, *UAL/ETEAPOT Proton EDM Benchmark Comparisons III: Dispersion, Longitudinal Dynamics and Synchrotron Oscillations,* BNL internal report, January 10, 2013

[6] Y.K. Semertzidis et al. *Spin Coherence Time Estimation in an All-Electric Field Using a Precision Tracking Simulation Program (DRAFT),* BNL internal report, August 28, 2012

[7] H. Wollnik, *Optics of Charged Particles,* Academic Press, Harcourt Brace Jovanovic, Publishers, 1987

[8] N. Malitsky, J. Talman, and R. Talman, *Appendix UALcode: Development of the UAL/ETEAPOT Code for the Proton EDM Experiment,* UAL/ETEAPOT documentation (frequently revised), August, 2012

[9] Storage Ring EDM Collaboration, *A Proposal to Measure the Proton Electric Dipole Moment with* 10^{-29} *e-cm Sensitivity,* especially Appendix 1. October, 2011